PCCP

PAPER

View Article Online
View Journal | View Issue

Cite this: *Phys. Chem. Chem. Phys.*, 2015, **17**, 18337

Fluorination-dependent molecular orbital occupancy in ring-shaped perfluorocarbons†

Tim Brandenburg,[ab] Tristan Petit,[a] Antje Neubauer,[a] Kaan Atak,[ab] Masanari Nagasaka,[c] Ronny Golnak,[ab] Nobuhiro Kosugi*[c] and Emad F. Aziz*[abc]

Received 3rd March 2015,
Accepted 17th June 2015

DOI: 10.1039/c5cp01254f

www.rsc.org/pccp

Perfluorocarbons are a family of molecules consisting mainly of carbon and fluorine atoms. They have interesting chemical properties and have diverse applications in biomedicine, physical chemistry and polymer science. In this work, carbon K-edge absorption and emission spectra of liquid decalin are presented and compared to perfluorodecalin. A comprehensive picture of the electronic structure of decalin is provided based on soft X-ray absorption and emission spectroscopies. Experimental data are compared to theoretical time-dependent density functional theory for the hydrocarbon, the perfluorocarbon and the stepwise fluorinated derivatives. We observed a molecular orbital change from unoccupied to occupied orbitals for perfluorodecalin, which was induced through the fluorination process.

1 Introduction

The family of perfluorocarbons has a wide range of applications in biomedicine and physical chemistry due to their extraordinary properties.[1,2] Many liquid perfluorocarbons are known to show high density, high viscosity as well as an especially high gas solubility, and are often chemically and biological inert.[3,4] Their ability to dissolve gases and their biological inertness are exploited in applications, such as tissue oxygenation[5–7] or post-operative treatment.[8,9]

The perfluoro effect, inherent to all perfluorocarbons, describes the energetic shifts of the spectral features upon complete fluorination of hydrocarbons.[10–13] This also led to a general rule for the dimensions of the energetic shifts depending on σ- or π-character of the molecular orbitals (MO).[11,12] Hence, this effect can be used for experimental orbital classification. In this context, a few experimental studies have already been performed in the 1970s.[11,12] Many of them were based on photoelectron and X-ray absorption (XA) spectroscopy.[10–14] Since then, more complex theoretical models[15] and the introduction of new experimental techniques[16–18] give opportunities to investigate perfluorocarbons.

Perfluorodecalin (PFD) is often studied as a general model system for perfluorocarbons. It exhibits the special chemical properties of perfluorocarbons[3,11,19,20] and is frequently used in applications.[5,7–9] In a previous study of the electronic structure of PFD weak intermolecular interactions and high inertness were traced back to a large energetic gap between the highest occupied MO (HOMO) and the lowest unoccupied MO (LUMO) and to the geometrical structure.[19]

Here we present experimental XA and X-ray emission (XE) data of the parent hydrocarbon decalin and compare them to former results for the perfluorocarbon PFD.[19] A discussion of the theoretically calculated absorption and emission spectra is also presented. We reveal the energetic shift induced by the perfluoro effect experimentally by XE measurements, which are shown here to give complementary results to the XA spectra. In addition, a systematic theoretical study for all stepwise fluorinated decalin derivatives was performed with the aim to gain clear insight into the mechanism of the perfluoro effect and the MO character of decalin and PFD.

2 Experimental and theoretical details

2.1 Materials and methods

Perfluorodecalin (PFD) and Decalin were obtained from Alfa-Aeser in a 50/50 *cis*/*trans* mixture with >95% purity for PFD and >98% purity for Decalin. Resonant inelastic X-ray scattering (RIXS) and XE spectra at the Decalin carbon K-edge were recorded using a liquid microjet setup[21,22] at the U41-PGM undulator beamline of BESSY II at Helmholtz-Zentrum Berlin[16] with a microjet diameter of around 14 μm. Detailed information about the end-station (LiXEdrom) is presented elsewhere.[21,23] The RIXS and XE measurements were performed using a Rowland-circle geometry spectrometer with a grating of 5 m radius of curvature and 1200 lines per mm. The detector, which is operated at a pressure of 10^{-9} mbar, consists of an MCP-stack, phosphorescent screen

[a] *Institute of Methods for Material Development, Helmholtz-Zentrum Berlin für Materialien und Energie, Albert-Einstein-Straße 15, 12489 Berlin, Germany. E-mail: emad.aziz@helmholtz-berlin.de*
[b] *Department of Physics, Freie Universität Berlin, Arnimallee 14, 14195 Berlin, Germany*
[c] *Institute for Molecular Science, Myodaiji, Okazaki 444-8585, Japan. E-mail: kosugi@ims.ac.jp*

† Electronic supplementary information (ESI) available. See DOI: 10.1039/c5cp01254f

and a CCD camera. The pressure in the experimental chamber is generally around 10^{-5} mbar. The beamline U41-PGM provides an excitation energy bandwidth of 0.1 eV at the energy of 300 eV for carbon excitations. The energy calibration and alignment of the RIXS and XE spectra was performed using the elastic scattering features.

XA spectra were measured by using a transmission-type liquid flow cell connected at soft X-ray undulator beamline BL3U at the UVSOR-III Synchrotron facility.[24] The details of the liquid flow cell are described elsewhere.[25,26] The liquid cell consists of four regions, which are separated by 100 nm thick Si_3N_4 membranes. Soft X-rays under vacuum (region I) pass through the buffer region filled with helium gas (region II) and the liquid thin layer (region III) and finally reach a photodiode detector in the last region filled with helium gas (region IV). A liquid sample is sandwiched between two Si_3N_4 membranes with pressed Teflon spacers set between the window frames of the membranes and can be substituted by other samples in combination with a tubing pump system. The thickness of the liquid layer can be controlled from 2000 to 20 nm by adjusting the helium pressure in the regions II and IV. The energy resolution of incident soft X-rays at C K-edge is set to 0.19 eV. XA spectra are based on the Beer–Lambert law, $\ln(I_0/I)$, where I_0 and I are the detection current through the cell without and with samples, respectively. The energetic alignment of the spectrometer was performed using CH_4 gas and its absorption line.

2.2 Theoretical methods

The presented theoretical calculations were carried out with the ORCA program package.[15] Molecular geometry optimizations were performed using the B3LYP[27,28] density functional method with the def2-TZVP basis set.[29,30] During the optimization calculations, the resolution of identity approximation[31–35] was used employing the def2-TZV/J basis set.[36] Due to the chiral character of the calculated molecules an optimization for each respective configuration was performed. The electron population was calculated using the Löwdin population analysis formalism. Transition energies and moments for the K-edges of both *cis* and *trans* configurations were calculated with time-dependent density functional theory (TD-DFT). The core-hole excited state calculations are based on the computation of the dipole length and dipole velocity formalisms. Additionally no intermolecular interaction effects in liquid phase are included. The presented X-ray emission spectra were predicted with a one-electron approach, based on the above described optimized geometries. K-edge absorption spectra were obtained from the calculated transition moments from both chiral contributions by applying a Gaussian type broadening of 0.8 eV.

The theory does not predict any significant difference between the X-ray spectra of *cis* and *trans* forms of the molecule. All molecular orbitals are subsequently shown from the *trans* configuration.

3 Results and discussion

The experimental carbon K-edge XA spectrum of decalin (Fig. 1C) reveals two peaks at 287.2 eV and 288.7 eV followed by a broad feature extending from 291 eV to 294 eV.

The general spectral shape of the XA spectrum of decalin can also be reproduced in shape and energetic position by theoretical gas phase calculations for a single molecule employing the density functional theory (DFT) algorithm for geometry optimizations and TD-DFT for spectral calculations on single molecules (for details see Theoretical methods). Nevertheless, the neglect of intermolecular interactions inside the liquid probably leads to the different intensity ratios for the two peaks at 287.2 eV and 288.7 eV by comparing theoretical and experimental data.

In Fig. 1C, the theoretical spectrum for all C sites (red line) was obtained through the sum of the spectra for the non-equivalent carbon sites. Additional calculations for the different carbon atom environments were derived in a similar manner as for PFD.[19] Note that the two different carbon atom sites in decalin only differ by the number of bound hydrogen atoms. Eight carbon atoms are bound to two carbon and two hydrogen atoms as nearest neighbors (dC), while the two carbon atoms connecting the rings (sC) are bound to three carbon atoms and one hydrogen atom as nearest neighbors. Hence, these two carbon sites should have a significantly different chemical environment. The corresponding theoretical spectra were obtained through the sum of the spectra for all dC and sC sites respectively and are shown in Fig. 1C and depict surprisingly a similar spectrum for dC and sC sites, in contrast to the findings for PFD.[19] In PFD the difference for the two carbon sites was mainly attributed to the slight net charge difference for dC and sC atoms (0.26–0.27 for dC and 0.16 for sC).[19] In contrast, for decalin the negative net charge on the carbon atoms is quite similar (0.21–0.23 for dC and 0.20 for sC), resulting in almost identical spectra. Additionally, we take note of the change from negative net charge for decalin carbons to positive net charge for PFD carbons, occurring due to the substitution of hydrogen to highly electronegative fluorine.

The experimental carbon K-edge XE spectra (Fig. 1B) are in good agreement with the calculated spectra (Fig. 1A). The spectra in Fig. 1B reveal an excitation-energy dependence in the range of 286.8–288.7 eV, where the high energy shoulder (β_4) at 279.6 eV emission energy gains intensity. Additionally, the spectral structure remains unchanged for excitation energies higher than 288.7 eV. This effect can be attributed to so-called tail excitation and vibronic coupling.[37,38]

The XE spectrum of PFD reveals three peaks consisting of a broad low energy peak around 275 eV and two high energy peaks.[19] By comparing to XE spectra of rather simple fluoromethanes[39] an influence of fluorine atoms to the high energy features were shown.[19] Subsequently the carbon K-edge emission spectrum of CH_4 should reveal similarities to decalin due to the absence of fluorine atoms and the sp^3-hybridized carbon character. Indeed, CH_4 shows one broad feature around 276.3 eV, which is an indicator for sp^3 hybridized carbon.[39] Furthermore, a glance at the spectra of C_2H_6 and C_3H_8 reveals an additional shoulder compared to the carbon XE spectra of CH_4 at around 274.8 eV.[40] This shoulder can be attributed to C–C bond interactions and coincides with the decalin β_2 structure at 274.6 eV in this work.

As expected, the decalin spectrum is more complex than simple fluorinated hydrocarbons, exhibiting a broad peak with two features around 278 eV and small energetic shifts. Anyhow, due to the

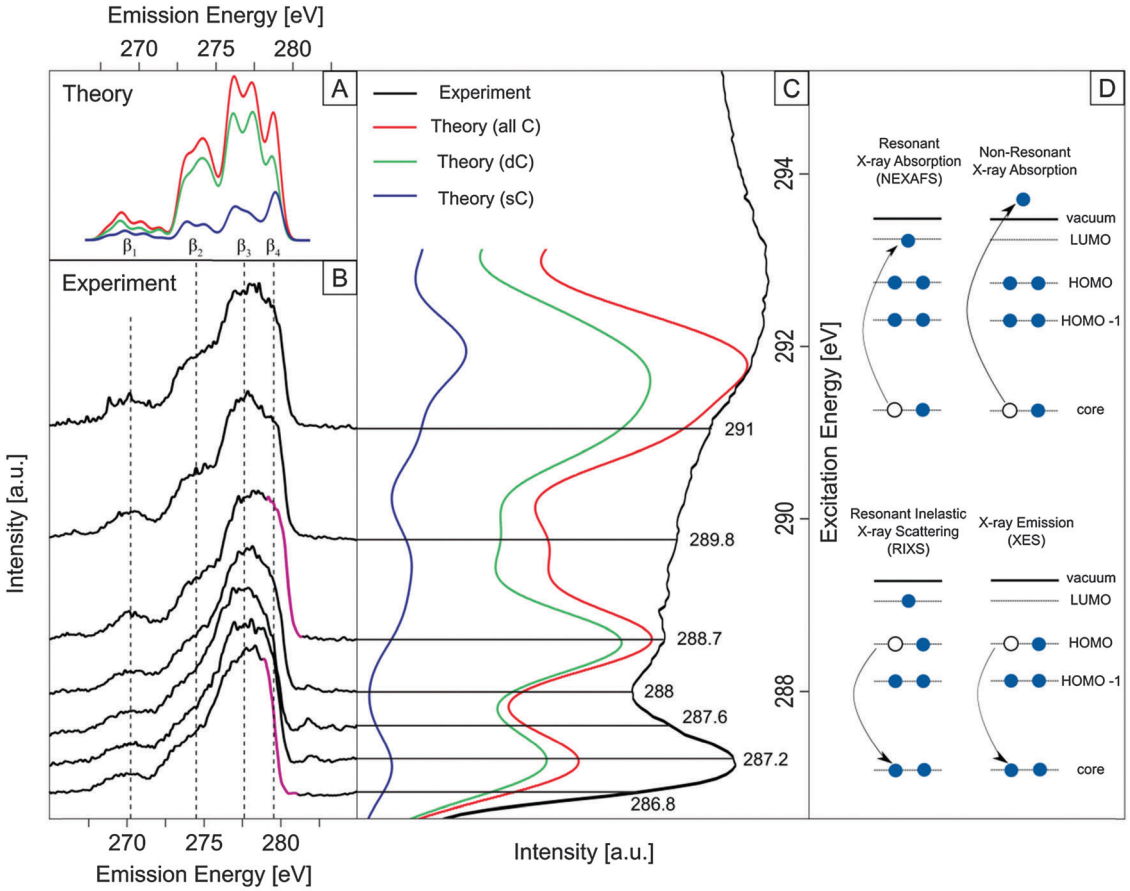

Fig. 1 Experimental and theoretical carbon K-edge X-ray emission (A, B) and X-ray absorption (C) data for decalin. Theoretically calculated data are shown for different carbon sites. The highlighted edges in the RIXS spectra (B) indicate the excitation-energy dependent spectral features. Additional information on the excitation processes for the different spectroscopies is provided (D).

phenomenological similarity to simple hydrocarbons, we can assign β_3 and β_4 as sp^3 hybridized carbon structures and the shoulder β_2 as resulting from C–C bond interactions.

Fig. 2A and 3A show the experimental carbon K-edge XA and XE spectra, respectively, for decalin and PFD and the calculated spectra for these molecules as well as for the stepwise fluorinated decalin derivatives (see also ESI†). The figures also visualize the shifts of the four main features for XA and the five main features for XE spectra. As mentioned above, according to the dimensions of the shifts for these features it is common to assign directly a σ- or π-character for the participating orbitals (~2–4 eV corresponds to σ, ~0–0.5 eV corresponds to π),[11,12] where π is of out-of-plane and diffuse (Rydberg-like) character, but not of anti-bonding character like π*. This is summarized in Table 1. We note that the XE spectra of PFD and decalin are dominated by σ type orbitals and that the first appreciable π contribution is in the XA region.

Features A and B_2 are special due to their disappearance in the spectra of PFD. All other calculated fluorocarbons show these features even though their intensity decreases with increasing number of F atoms. Furthermore, these features do not have corresponding PFD orbitals for the absorption process, but for the emission process. We additionally note that B_2 only loses its dC contribution to the spectrum, while the sC contribution remains of the same intensity (see Fig. S1, ESI†).

Features B_2, Γ and Δ_1 can only be assigned to both σ- and π-orbital character since the observed energetic shift is in the range known for strong σ–π-hybridization. According to the relative high values of 1.3 eV and 1.4 eV for B_2 and Δ_1, respectively, a larger contribution of σ-character for these features can be assumed in comparison to Γ with a value of 0.9 eV for the energetic shift.

Complementary to the XA spectra, features δ and ε for the XE spectra (Fig. 3A) require special attention. They do not exist in decalin but appear upon fluorination. This coincides favorably with the disappearance of the absorption features A and B_2. Simultaneously, both the XA features (A, B_2) and the XE features (δ, ε) originate from similar MOs and we can assume a switch from unoccupied to occupied orbital region. The differences of the MOs have to be taken into account under the assumption of the intrinsic differences between occupied and unoccupied orbitals, like the electronic nodal planes and electron distribution. Accordingly, the change from unoccupied to occupied orbitals (A to δ and B_2 to ε) occurs due to the enormous number of additional orbitals and the different partial charge distributions based on the substitution of hydrogen by electronegative fluorine. The stronger electronegativity results in a depopulation of most carbon orbitals (see the population analysis *vide supra*), giving dominance to fluorine signals in the XE spectra.[19] The transformation of the previous pure carbon orbitals with

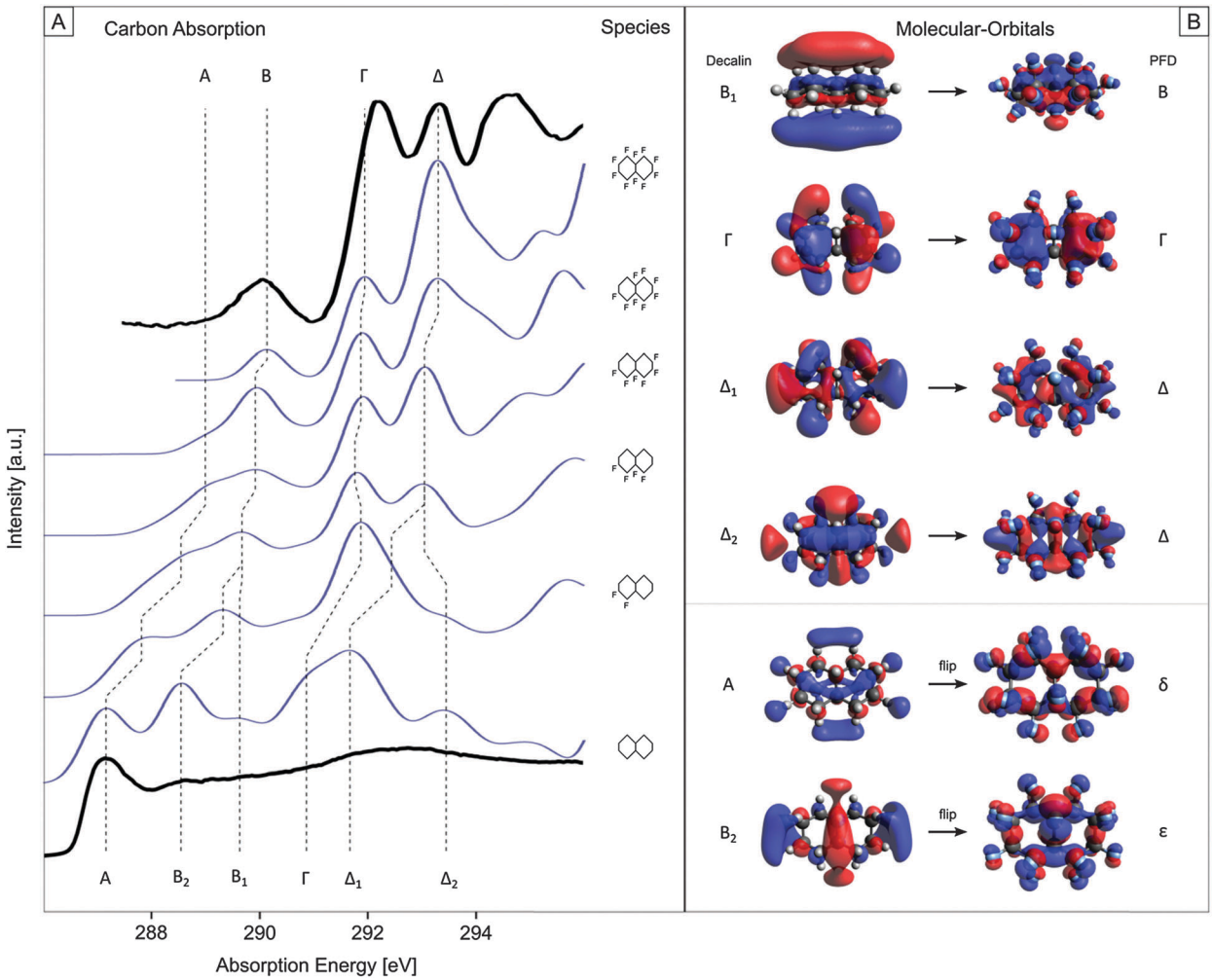

Fig. 2 (A) Experimental (black lines) and calculated (blue lines) carbon K-edge X-ray absorption spectra for decalin and PFD as well as calculated spectra for stepwise fluorinated decalin derivatives. Dashed lines indicate the shifts of the spectral features. (B) MOs for decalin and PFD corresponding to the shifting features are labeled in (A).

fluorine contribution can therefore lead to an energetic shift of the occupied orbitals due to the increase in fluorine character.

In addition to the orbital change, a σ-shifting effect is observed. This σ-shifting effect is known for hydrocarbons, where a C–C bond length increase is accompanied by a shift of σ-features to lower energies.[41,42] The average C–C bond length was here calculated to be 1.565 Å for PFD and 1.533 Å for decalin. Note, the C–C bond length in partially fluorinated compounds is slightly higher for bonds including fluorine substituted carbon atoms than for only hydrogen substituted carbon atoms (around 1.545–1.565 Å *vs.* 1.529–1.534 Å). Hence, the σ shifting has only impact where fluorine substituted carbon atoms are involved. Consequently, the orbital change is strongly affected by σ shifting, supporting and strengthening the orbital rearrangement.

The aforementioned energetic shifts and assignments also coincide with the observations of PFD RIXS measurements, in which the feature δ is a mixture of sC and dC carbon sites and ε of only dC carbon sites.[19]

As mentioned above, in a previous work[19] we found that PFD has a large HOMO–LUMO gap supposedly of importance for the chemical inertness and properties of PFD. By our present data on decalin and the partially fluorinated hydrocarbons, we gain insight into the mechanism behind this. For a precise estimation of the gap, the energetic alignment of the different experimental spectra is crucial. A detailed description on the alignment can be found under experimental methods. Our data supports a significant increase of the gap for the last fluorination step ($C_{10}F_{26}H_2$ to $C_{10}F_{28}$). For this step, the gap increases by 1.2 eV due to the orbital change of the features A and B_2 into the occupied orbital region additionally to the systematic energy shift for these features. This increases the relative inertness according to the frontier orbital model[43] and reveals the critical impact of the orbital change on the inertness of the perfluorinated molecule.

Additionally, parallels between the observed orbital change and molecule enhancement methods through fluorine treatment should be discussed.[44,45] The observations are similar with respect to the observed changes in the MO structure and the resulting changes in chemical character.[44–47] To enhance the mechanistic understanding and involvement of the orbital change in these methods and molecules, further research on chain structured and

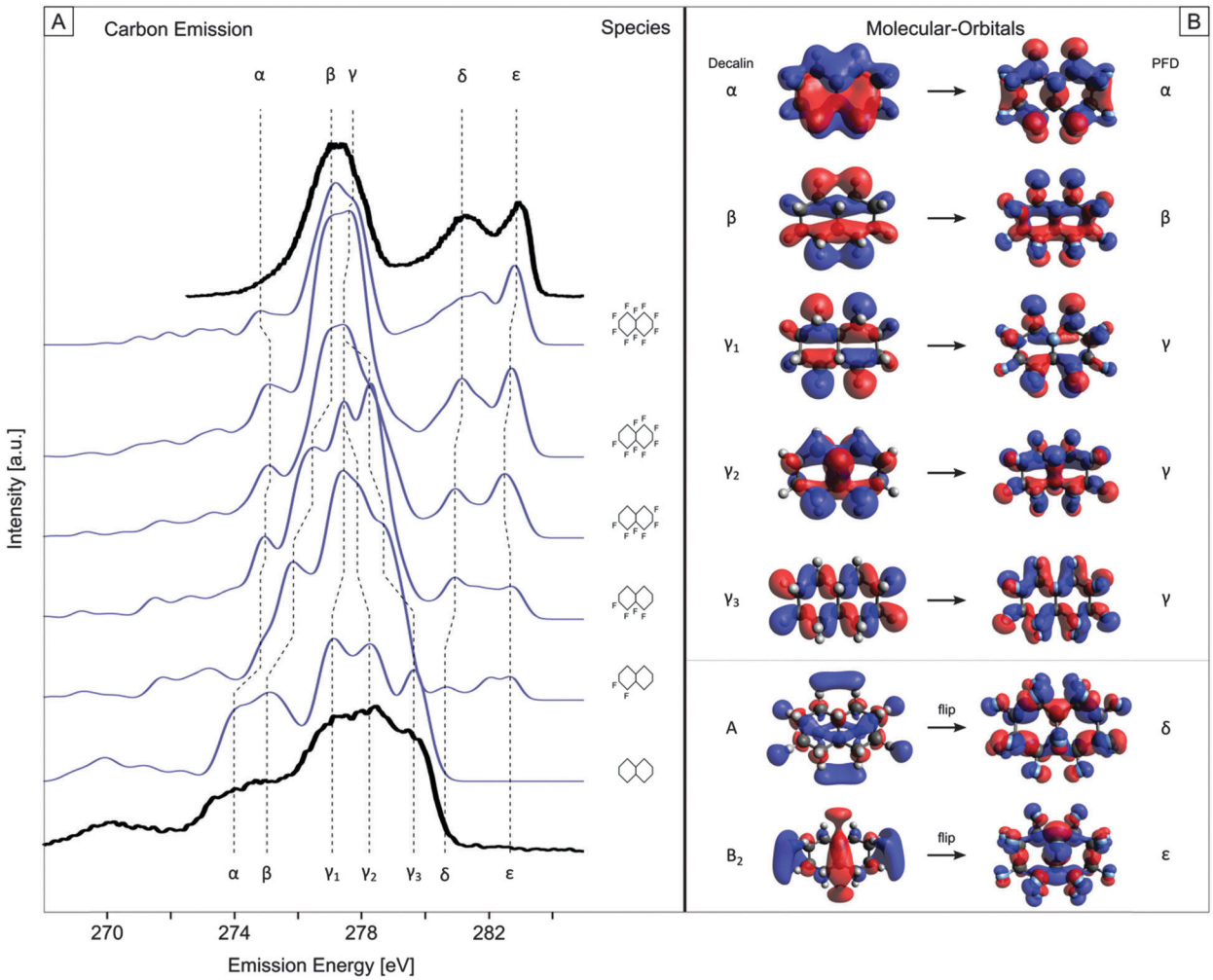

Fig. 3 (A) Experimental (black lines) and calculated (blue lines) carbon K-edge X-ray emission spectra for decalin and PFD[19] and calculated spectra for stepwise fluorinated decalin derivatives. Dashed lines indicate the shifts of the spectral features. (B) MOs for decalin and PFD corresponding to the shifting features are labeled in (A).

Table 1 Energetic shifts and derived MO character for the XA and XE features

XA characters and shifts			XE characters and shifts		
Feature	Energetic shift upon complete fluorination [eV]	Orbital character	Feature	Energetic shift upon complete fluorination [eV]	Orbital character
A	1.8	σ	α	0.9	Not distinguishable
B_1	0.3	π	β	2.1	σ
B_2	1.3	Not distinguishable	γ_1	0.7	σ/not distinguishable
Γ	0.9	Not distinguishable	γ_2	0.6	Not distinguishable
Δ_1	1.4	Not distinguishable	γ_3	1.9	σ
Δ_2	0.1	π	δ	0.2	σ
			ε	0.1	Not distinguishable

more complex perfluoro compounds is in progress and will hopefully deliver a more general understanding of these findings.

4 Conclusions

In summary, we presented fundamental insight into the energetic shift induced by fluorination, the so-called perfluoro effect, and a comprehensive picture of the electronic structure of decalin as the parent hydrocarbon molecule for the recently investigated perfluorodecalin[19] based on XA, XE and RIXS spectroscopic data. In addition, DFT calculations for decalin, perfluorodecalin and stepwise fluorinated decalin derivatives were performed. We observed a change in occupancy of MOs occurring for the fluorinated hydrocarbons when reaching complete fluorination in PFD. This MO alteration may be one of the main reasons for

the chemical and biological inertness of the ring-shaped perfluorodecalin compared to decalin and the corresponding partially fluorinated hydrocarbons.[3,4] Interestingly, the orbital change assigned to the A and B_2 feature in the XA spectra could also be observed in the XE spectra for the features δ and ε in a complementary way. To the best of our knowledge, the observability of the perfluoro effect *via* XE spectra was confirmed for the first time, and the orbital change originating from unoccupied decalin to occupied PFD MOs was also discussed in relation to the well-known high electronegativity of fluorine atoms. Hence, the validity of this concept and its extension to linear and also larger perfluoro systems is of particular interest for a better understanding of the special properties of perfluoro compounds and their application development.

Acknowledgements

This work was supported by the Helmholtz-Gemeinschaft *via* the young investigator fund VH-NG-635. Part of this work was financially supported by the European Research Council grant No. 279344. Tristan Petit acknowledges the Alexander von Humboldt foundation for financial support. Kaan Atak would like to acknowledge the financial support of the Einstein Foundation Berlin for the postdoctoral scholarship in the Aziz team. This work is supported by JSPS Grants-in-Aid for Scientific Research (No. 26248010). We acknowledge the staff members of the UVSOR-III Synchrotron facility for their kind support.

References

1 J.-A. Ma and D. Cahard, *Chem. Rev.*, 2004, **104**, 6119–6146.
2 *Selective Fluorination in Organic and Bioorganic Chemistry*, ed. J. T. Welch, American Chemical Society, Washington, DC, 1991, vol. 456.
3 M. A. Hamza, G. Serratrice, M. J. Stebe and J. J. Delpuech, *J. Am. Chem. Soc.*, 1981, **103**, 3733–3738.
4 A. M. A. Dias, M. Freire, J. A. P. Coutinho and I. M. Marrucho, *Fluid Phase Equilib.*, 2004, **222–223**, 325–330.
5 K. C. Lowe, *Blood Rev.*, 1999, **13**, 171–184.
6 M. C. Papo, P. R. Paczan, B. P. Fuhrman, D. M. Steinhorn, L. J. Hernan, C. L. Leach, B. A. Holm, J. E. Fisher and B. A. Kahn, *Crit. Care Med.*, 1996, **24**, 466–474.
7 P. R. Lyunch, L. J. Krasner, T. Vinciquerra and T. H. Shaffer, *Undersea Biomed. Res.*, 1989, **16**, 275–281.
8 M. Velikay, A. Wedrich, U. Stolba, P. Datlinger, Y. Li and S. Binder, *Am. J. Ophthalmol.*, 1993, **116**, 565–570.
9 F. Bottoni, G. Bailo, P. Arpa, A. Prussiani, M. Monticelli and V. de Molfetta, *Ophthalmic Surg.*, 1994, **25**, 365–373.
10 P. Decleva, M. Stener, D. M. P. Holland, A. W. Potts and L. Karlsson, *J. Phys. B: At., Mol. Opt. Phys.*, 2007, **40**, 2939.
11 C. R. Brundle, M. B. Robin, N. A. Kuebler and H. Basch, *J. Am. Chem. Soc.*, 1972, **94**, 1451–1465.
12 C. R. Brundle, M. B. Robin and N. A. Kuebler, *J. Am. Chem. Soc.*, 1972, **94**, 1466–1475.
13 M. B. Robin, I. Ishii, R. McLaren and A. P. Hitchcock, *J. Electron Spectrosc. Relat. Phenom.*, 1988, **47**, 53–92.
14 I. Ishii, R. McLaren, A. P. Hitchcock, K. D. Jordan, Y. Choi and M. B. Robin, *Can. J. Chem.*, 1988, **66**, 2104–2121.
15 F. Neese, *Wiley Interdiscip. Rev.: Comput. Mol. Sci.*, 2012, **2**, 73–78.
16 C. Jung, F. Eggenstein, S. Hartlaub, R. Follath, J. S. Schmidt, F. Senf, M. R. Weiss, T. Zeschke and W. Gudat, *Nucl. Instrum. Methods Phys. Res., Sect. A*, 2001, **467–468**(Part 1), 485–487.
17 M. Nagasaka, H. Yuzawa, T. Horigome, A. P. Hitchcock and N. Kosugi, *J. Phys. Chem. C*, 2013, **117**, 16343–16348.
18 F. Gel'mukhanov and H. Ågren, *Phys. Rep.*, 1999, **312**, 87–330.
19 T. Brandenburg, M. Agåker, K. Atak, M. Pflüger, C. Schwanke, T. Petit, K. M. Lange, J.-E. Rubensson and E. F. Aziz, *Phys. Chem. Chem. Phys.*, 2014, **16**, 23379–23385.
20 E. P. Wesseler, R. Iltis and L. C. Clark Jr., *J. Fluorine Chem.*, 1977, **9**, 137–146.
21 K. M. Lange, R. Könnecke, S. Ghadimi, R. Golnak, M. A. Soldatov, K. F. Hodeck, A. Soldatov and E. F. Aziz, *Chem. Phys.*, 2010, **377**, 1–5.
22 K. M. Lange, M. Soldatov, R. Golnak, M. Gotz, N. Engel, R. Könnecke, J.-E. Rubensson and E. F. Aziz, *Phys. Rev. B: Condens. Matter Mater. Phys.*, 2012, **85**, 155104.
23 K. M. Lange, R. Könnecke, M. Soldatov, R. Golnak, J.-E. Rubensson, A. Soldatov and E. F. Aziz, *Angew. Chem.*, 2011, **123**, 10809–10813.
24 T. Hatsui, E. Shigemasa and N. Kosugi, in *AIP Conference Proceedings*, AIP Publishing, 2004, vol. 705, pp. 921-924.
25 M. Nagasaka, T. Hatsui, T. Horigome, Y. Hamamura and N. Kosugi, *J. Electron Spectrosc. Relat. Phenom.*, 2010, **177**, 130–134.
26 M. Nagasaka, K. Mochizuki, V. Leloup and N. Kosugi, *J. Phys. Chem. B*, 2014, **118**, 4388–4396.
27 A. D. Becke, *Phys. Rev. A: At., Mol., Opt. Phys.*, 1988, **38**, 3098–3100.
28 A. D. Becke, *J. Chem. Phys.*, 1993, **98**, 5648–5652.
29 A. Schäfer, H. Horn and R. Ahlrichs, *J. Chem. Phys.*, 1992, **97**, 2571–2577.
30 F. Weigend and R. Ahlrichs, *Phys. Chem. Chem. Phys.*, 2005, **7**, 3297.
31 E. J. Baerends, D. E. Ellis and P. Ros, *Chem. Phys.*, 1973, **2**, 41–51.
32 B. I. Dunlap, J. W. D. Connolly and J. R. Sabin, *J. Chem. Phys.*, 2008, **71**, 3396–3402.
33 O. Vahtras, J. Almlöf and M. W. Feyereisen, *Chem. Phys. Lett.*, 1993, **213**, 514–518.
34 K. Eichkorn, O. Treutler, H. Öhm, M. Häser and R. Ahlrichs, *Chem. Phys. Lett.*, 1995, **240**, 283–290.
35 K. Eichkorn, F. Weigend, O. Treutler and R. Ahlrichs, *Theor. Chem. Acc.*, 1997, **97**, 119–124.
36 F. Weigend, *Phys. Chem. Chem. Phys.*, 2006, **8**, 1057.
37 P. Skytt, J. Guo, N. Wassdahl, J. Nordgren, Y. Luo and H. Ågren, *Phys. Rev. A: At., Mol., Opt. Phys.*, 1995, **52**, 3572–3576.

38 J. Guo, *X-Rays in Nanoscience: Spectroscopy, Spectromicroscopy, and Scattering Techniques*, John Wiley & Sons, 2011.
39 P. Glans, R. E. L. Villa, Y. Luo, H. Agren and J. Nordgren, *J. Phys. B: At., Mol. Opt. Phys.*, 1994, **27**, 3399.
40 R. Manne, *J. Chem. Phys.*, 1970, **52**, 5733–5739.
41 A. P. Hitchcock, D. C. Newbury, I. Ishii, J. Stöhr, J. A. Horsley, R. D. Redwing, A. L. Johnson and F. Sette, *J. Chem. Phys.*, 1986, **85**, 4849–4862.
42 F. Sette, J. Stöhr and A. P. Hitchcock, *J. Chem. Phys.*, 1984, **81**, 4906–4914.
43 K. Fukui, T. Yonezawa and H. Shingu, *J. Chem. Phys.*, 1952, **20**, 722–725.
44 A. Tressaud, E. Durand, C. Labrugère, A. P. Kharitonov and L. N. Kharitonova, *J. Fluorine Chem.*, 2007, **128**, 378–391.
45 R. G. Haverkamp and B. C. C. Cowie, *Surf. Interface Anal.*, 2013, **45**, 1854–1858.
46 J. Guo, P. Resnick, K. Efimenko, J. Genzer and J. M. DeSimone, *Ind. Eng. Chem. Res.*, 2007, **47**, 502–508.
47 L. J. Gamble, B. Ravel, D. A. Fischer and D. G. Castner, *Langmuir*, 2002, **18**, 2183–2189.